Asian Journal of Advances in Research

4(1): 380-397, 2021

REMOVAL OF METHYLENE BLUE DYE USING COPPER OXIDE/CARBOXYMETHYL CELLULOSE NANOCOMPOSITE: KINETIC, EQUILIBRIUM AND THERMODYNAMIC STUDIES

W. A. ALBOKHEET[1], M. GOUDA[1*] AND Y. ALFAIYZ[1]

[1]Department of Chemistry, College of Science, King Faisal University, Al-Ahsa, 31982, Saudi Arabia.

AUTHORS' CONTRIBUTIONS

This work was carried out in collaboration among all authors. Author WAA conducted the practical part and wrote the original draft. Professor Author MG supervised the practical work, corrected the manuscript and submitted the manuscript. Author YA read and corrected the manuscript. All authors read and approved the final manuscript.

Received: 20 March 2021
Accepted: 25 May 2021
Published: 26 May 2021

Original Research Article

ABSTRACT

In this study, copper oxide / Carboxymethyl cellulose (CuO-CMC) nanocomposite was successfully synthesized by the co-precipitation method in presence of $NaBH_4$ as a reducing agent followed by thermal treatment using Muffle furnace at 300^{o}C, which involves the immobilization of copper oxide nanoparticles (Cu NPs) onto Carboxymethyl cellulose (CMC) structure. Synthesized CuO/CMC nanocomposite was characterized using Fourier transform infrared spectroscopy (FT-IR), Scanning electron microscope (SEM) coupled with Energy Dispersive X-ray analysis (EDX) as well as Transmission electron microscope (TEM). Crystallography of the synthesized nanocomposite was characterized using X-ray diffraction (XRD) as well. The nanocomposite was applied as an effective adsorbent to remove the organic pollutant such as methylene blue (MB) dye from its solution. Different factors affecting the dye removal such as initial dye concentration (3-15 mg/L), contact time (0-48 h), temperature (298-338 K), adsorbent dosage (2-10 mg), and pH (2-12) were evaluated. The maximum removal efficiency was observed to be (100, 100, 92, 86 %) for the initial concentration of MB (3, 7, 11, 15 mg/L) respectively with an adsorbent dosage (2.5 mg) after 48 hours. The experimental data exhibit that the adsorption behavior of CuO-CMC nanocomposite followed the pseudo 2nd order and the Langmuir isothermal model. Furthermore, the thermodynamics results suggested that the spontaneous nature and endothermic of the adsorption process.

Keywords: Copper oxide nanoparticles; carboxymethyl cellulose; nanocomposites; methylene blue; adsorption.

1. INTRODUCTION

Dyes are conventionally used for coloring products in industries, such as plastic, paper, leather, and textile. During the coloration process, a substantial amount of colored wastewater is generated, which leads to danger to human and aquatic life because the waste dyes can prevent light penetration and interfere with photosynthetic processes. Among these dyes is methylene blue [$C_{16}H_{18}ClN_3S$-(MB)], which is a cationic dye and extensively used in many industries, such as cosmetics, pharmaceutical, and food industries. It is worth noting that, the dye leads to permanent injury to the eyes and difficulty in

**Corresponding author: Email: mgoudaam@kfu.edu.sa;*

breathing, burning sensation, vomiting, and nausea when it is inhaled or ingested orally. Therefore, it must be removed from contaminated water [1,2]. Numerous techniques have been applied to remove dyes from wastewaters including photo-degradation [3], advanced oxidation processes [4], adsorption [5], coagulation, and flocculation [6] and supported liquid membrane technologies [7]. Some of these techniques have a weakness, for instance, low effectiveness, complicated design, high cost, and toxic products after degradation of MB. However, much of previous research reported that the adsorption technique is customarily preferred because of its higher removal capability with the ability to uptake MB at different concentrations and pH, proficient action under ambient conditions, eco-friendly and lower cost [8,9].

Furthermore, several attempts have been applied to remove the MB by effective adsorbents. Kuang et al. prepared the modified-activated carbon (AC) with an excessive elimination of MB from wastewater [10]. Moreover, Venkatesha et al. have prepared graphene oxide-Fe3O4 nanocomposite to remove MB and Rhodamine B dyes with high adsorption capacity [11]. Due to the high cost, non-biodegradable, difficulty to recover, and may cause pollution of these of materials, encouraged the researchers to synthesis adsorbents with good effect, low cost and non-harmful. Recently, the alternative and unpretentious approach that attracted researchers for water treatment is nanotechnology [12]. Metal oxide has significant attention, including copper oxide nanoparticles (CuO NPs) due to their distinctive properties, and stability which are more stable than other copper suboxides such as Cu2O [13]. CuO NPs have interesting applications in many fields such as nano-catalysis [14], nano-fluids [15], sensors [16], superconductors [17], antimicrobial [18] and energy storage systems [19]. Furthermore, CuO NPs can be exhibited an excellent result to remove MB, which is inexpensive, low toxicity, and abundant with short reaction time under not cruel conditions [12]. Hatem et al. and Mustafa et al. were prepared CuO NPs successfully and they exhibited the impressive elimination of MB dye molecules from wastewater [20, 21]. Generally, nanosized metals are unstable and tend to aggregate, and to overcome the aggregation of nanoparticles, the immobilization of metal NPs onto materials as support is the most effective concept [22]. Carbon is one of the support materials for metal nanoparticles and has great attention because of its advantages such as superb thermal, large electron-storage capacity, high surface area, and good stability. Kamal et al. and Mahdie et al. were synthesized copper oxide-Single-walled Carbon Nanotubes nanocomposite and Cu-based metal-organic framework (MOF) modified by sulfonate groups respectively and applied to eliminate MB dye from an aqueous solution [23, 24].

Furthermore, CuO NPs were synthesized by various methods, such as sol-gel [25], hydrothermal [26], chemical vapor deposition [27], sputtering [28], laser ablation [29] and co-precipitation [30]. Among these methods, the co-precipitation method is the most widely used because of its simplicity and low cost [13].

Moreover, biopolymers are promising and important building blocks for high-performance polymer nanomaterials, especially in terms of sustainability, efficiency, biodegradability, and environmental friendliness [31]. In general, the incorporation of metal oxide NPs into cellulose is an interesting way to improve the properties of materials that could act as a platform in the treatment of water. Moreover, the fabrication and application of metal oxides-cellulose nanocomposites in water treatment minimize the potential risks associated with the metal oxide NPs and the sorbent's properties are enhanced due to the NPs are dispersed through the functional groups of cellulose without aggregation. In addition, cellulose derivatives are also contributed to remediate the metal ions from wastewater [32]. Therefore, cellulose is used as a support or an adsorbent to remove the dyes according to its powerful mechanical features and eco-friendly resource. Furthermore, it can easily be chemically modified with various functional groups [33,34]. Recently, Diana et al. have been prepared the cross-linked dicarboxymethyl cellulose and its application to remove MB dye [35].

The aim of this study is to prepare copper oxide-carboxymethyl cellulose (CuO-CMC) nanocomposite and its application to remove methylene blue dye from water solution. The nanocomposites will be prepared by the co-precipitation method using $NaBH_4$ as a reducing agent. The synthesized nanocomposites will be characterized by FT-IR, XRD, SEM coupled with EDX and TEM spectroscopy. The influences of the initial concentration of MB, contact time, adsorbent dosages, temperature, and pH of the solution will be investigated. Lastly, the adsorption performance of MB was studied by using the adsorption of kinetics, isotherm models, and thermodynamic.

2. MATERIALS AND METHODS

2.1 Materials

Cellulose powder $(C_6H_{10}O_5)_n$, copper nitrate trihydrate ($CuN_2O_6.3H_2O$ 98%), sodium borohydride (98%), monochloroacetic acid (99%), methylene blue (Mw

373.7 g/mole), ethanol (99.9%), 2 propanol (99.8%) and sodium hydroxide (98%) were obtained from Sigma-Aldrich US Co. All the chemicals were used without further purification and all solutions were prepared using distilled water.

2.2 Synthesis of CuO-CMC Nanocomposite

In brief, CMC was prepared according to the procedure described by Khalil et al. [36] as follows: in a glass bottle (1mole) of cellulose was mixed with (1mole) of sodium hydroxide in the presence of water: isopropanol 3:3 (v/v) for 10 min. In the water bath, (1mole) of monochloroacetic acid was added dropwise to the mixture at 80^{o}C for 3 h. The neutralization step was occurred by adding 5 drops of conc. HCl. Then, the final product was washed with an isopropanol/water mixture (70:30) using Soxhlet for 24 h. After that, the sample was dried at 70^{o}C in an oven. The degree of substitution of prepared CMC was 0.58. The in situ deposition of CuO NPs into CMC structure was carried out according to the reported method [37] as follows: CMC (0.5 g) was added to 50 ml of copper nitrate trihydrate aqueous solution (0.01M) in Ultrasonic bath sonication for 30 min. The prepared mixture was transferred to a mechanical stirrer and $NaBH_4$ (1M) was added gradually with continuous stirring. The prepared sample was filtered, washed with distilled water, and then dried at 60^{o}C for 1 h. The dried sample was transferred into a Muffle furnace at 300^{o}C for 24 h.

2.3 Characterization

Synthesized CuO-CMC nanocomposite was characterized using Fourier transform infrared spectroscopy (FT-IR, Agilent Technologies, cary630, Malaysia) in the range of 400 to 4000 cm^{-1}. Crystallographic properties of the prepared nanocomposite were characterized by X-ray diffraction (XRD, Rigaku, Tokyo, Japan) was carried out with Cu-Kα radiation (λ = 0.154 nm) at 40 kV and 30 mA and the ranging of 2θ from 5° to 75°. The thermal stability of the prepared samples was investigated using a thermogravimetric analyzer (TGA), TA instrument model (Q 500-USA). Scanning electron microscopy equipped with an energy dispersive X-ray diffraction (SEM-EDX type JXA-840 an electron probe microanalyzer-JOEL) was used to study the surface morphology and elemental analysis of the prepared nanocomposites. The size diameter and particle size distribution of the prepared nanocomposites were characterized using transmission electron microscopy (TEM ZEISS-EM-10-GERMANY).

2.4 Methylene Blue Adsorption

Synthesized CuO-CMC nanocomposite was used to remove methylene blue according to [38]. as follows: The standard curve of methylene blue was prepared by using different concentrations (3, 7, 11, 15 mg/L) and the absorbance of each concentration was measured using a UV-Vis spectrophotometer (GENESYS 10S UV VIS, Thermo Scientific, Madison) at maximum wavelength λ_{max}= 660 nm. Synthesized nanocomposites (2-10 mg) were added to the solution of MB with different initial concentrations (3-15 mg/L) for different adsorption times (0-48 h) at different adsorption temperatures (25-65^{o}C) and pH values (2-12). The investigations were rehashed three times and CMC blank was performed, and the average concentration and average standard deviations were accounted. These experiments were conducted to investigate the isotherm and thermodynamic adsorption with 3 mg/L of MB initial concentration. Furthermore, the Kinetics of adsorption was carried out as follows: MB initial concentrations were (3-15 mg/L), pH was 5.5, time was 48 h, and 2.5 mg of the nanocomposite. The removal efficiency percent of MB was determined according to the remaining concentration after treatment. The dye removal percentage (%) was calculated by the following equation:

$$Removal\ percentage = \frac{(C_o - C_t)}{Co} \times 100 \quad (1)$$

where C_o is the MB initial concentration and C_t is the MB final concentration (mg/L) at a definite time. Furthermore, the amount of methylene blue adsorbed onto nanocomposite Q (mg of dye/ gm of adsorbent) was calculated according to following equation:

$$Q\,(mg/g) = \frac{(C_o - C_t)V}{M} \quad (2)$$

where V is the volume (L) of MB solution and M is the mass of nanocomposites (g).

3. RESULTS AND DISCUSSION

3.1 Synthesis of CuO-CMC Nanocomposite

CMC was prepared through two reaction steps; alkalization reaction follows by etherification reaction. In the alkalization process, the cellulose was treated with NaOH at room temperature in presence of inert solvent (isopropanol), which acts as a swelling agent to facilitate the penetration to the crystalline structure of cellulose. It solvates the hydroxyl groups and thus makes them available for etherification

reaction. In the etherification step, the sodium cellulosate was reacted with monochloroacetic acid to form carboxymethyl cellulose [39]. CMC-Cu^{2+} was formed by the metathesis of copper nitrate trihydrate aqueous solution and CMC at room temperature. The blue precipitate was formed indicated that the successful formation of CMC-Cu^{2+} via the ion exchange process [40]. Prepared CMC-Cu^{2+} was treated with (1M) of $NaBH_4$ aqueous solution, the blue color of the precipitate was changed to black color which indicates the formation of Cu nanoparticles according to the following equation (3) [41]:

$$Cu^{2+} + 4BH_4^- + 12H_2O \rightarrow 2\ Cu^0 + 14H_2 + 4B(OH)_3 \quad (3)$$

Copper NPs was converted into CuO NPs with thermal processing at 300°C. The following proposed reaction mechanism of CuO-CMC nanocomposite formulation as shown in Fig. 1.

3.2 Characterization of the Synthesized Nanocomposite

3.2.1 FT-IR spectra

FT-IR was used to confirm the existence of copper oxide nanoparticles in cellulose structure. Fig. 2 shows the FT-IR spectra of A) Cellulose, B) CMC and C) CuO-CMC nanocomposites. Fig. 2A shows FTIR of native cellulose and the data show that the main band of OH groups at 3280 cm^{-1} and the bands at 2894 cm^{-1} due to C-H vibration. The characteristic bands at 1428, 1027, and 892 cm^{-1} indicated CH_2 bending, C-O-C pyranose ring vibration, and C-O-C stretching the β (1→4)-glycosidic linkage between the glucose units, respectively [42]. Fig. 2B shows the FT-IR spectra of thermal treated CMC at 300°C with increasing in width which corresponding to OH stretching vibration and there are two peaks at 1725 and 1628 cm^{-1}, which referred to the C=O group and stretching vibration of (COO-) group, respectively [43]. On the other hand, after generating of NPs onto CMC the peaks related to OH stretching and C-O-C pyranose ring vibration are disappear. Moreover, the bands of C=O and COO- groups stretching vibration were shifted from 1725, 1628 to 1704, 1572 cm^{-1}, respectively with low intensity, implying coordination of COO- with Cu^{2+}. In addition to the characteristic peaks for the CuO-CMC spectrum obvious a weak peak at 433 cm^{-1} that assigned to CuO vibration, proved the presence of CuO NPs on the CMC surface [44].

3.2.2 XRD analysis

In order to study the effect of CuO nanoparticles on the crystallinity of CMC, X-ray diffraction (XRD) analysis was used. Fig. 3A shows the XRD patterns for CMC, the main characteristic peak was observed at 2θ of 22.69 ° with low intensity, which is attributed to (200) planes of the crystalline structure of CMC. While Fig. 3B shows the XRD pattern of CuO-CMC nanocomposite this figure shows sharp and strong peaks at 2θ of 32.81, 36.66, 38.30, 54.31, 61.26, and 65.60°, which are assigned to the (110), (111), (200), (020), (113) and (002) crystal planes respectively (JCPDS, 45-0397). In addition, two characteristic peaks were observed at 43.62° (-111) and 73.75 (220) which corresponding to the copper metal this is attributed to a small portion of copper metals that did not convert into an oxidation state after thermal treatment at 300°C. The average crystallite size of copper oxide NPs was calculated using Scherrer's formula (4) and it was found 25-57 nm.

$$D_{nm} = \frac{k\,\lambda}{\beta\ cos\theta} \quad (4)$$

where D is crystallite size (nm), k is Scherrer constant= 0.89, λ is the X-ray wavelength= 0.15425 nm, β is the full width at half maximum of the peak (FWHM) and θ is the Bragg angle [33].

3.2.3 Thermogravimetric analysis (TGA)

Studying the thermal characteristics of strengthening ingredients is significant to distinguish their application as bio-composite handling at extraordinary temperatures [45]. Fig. 4 shows TGA investigation, and derivative thermogram (DTG) curves for native cellulose (Cell-OH), CuO/CMC, and CMC. Thermal degradation of Cell-OH), CuO/CMC, and CMC provided a primary weight residual in the variety of 50–200°C because the vaporization of lightly assured humidity on the surface of the specimens [46] (Li et al., 2009; Rosa et al., 2012). Cell-OH), CuO/CMC, and CMC samples display two-step degradation. Onset temperature (T_{onset}) of the CuO/CMC and CMC started at 250°C respectively, while the onset temperature of pure cellulose started at 345°C, which are minor temperatures matched to the thermal degradation of pure cellulose. From Fig. 4, the breakdown temperatures band for individual specimens can be understood in the derivative weight loss curve (DTGA curve). The maximum decomposition peak temperature of CuO/CMC and CMC is observed at 350°C, while, Cell-OH is observed at 360°C; at these temperatures, the cellulose will decompose affording to Jonoobi et al. [47]. The maximum degradation temperature of Cell-OH, CuO/CMC, and CMC is understood to be owing to a strong decrease in molecular weight of the samples, which makes them more liable to decompose when the temperature rises. It is also expected that hydrolysis of cellulose not only dissolves the

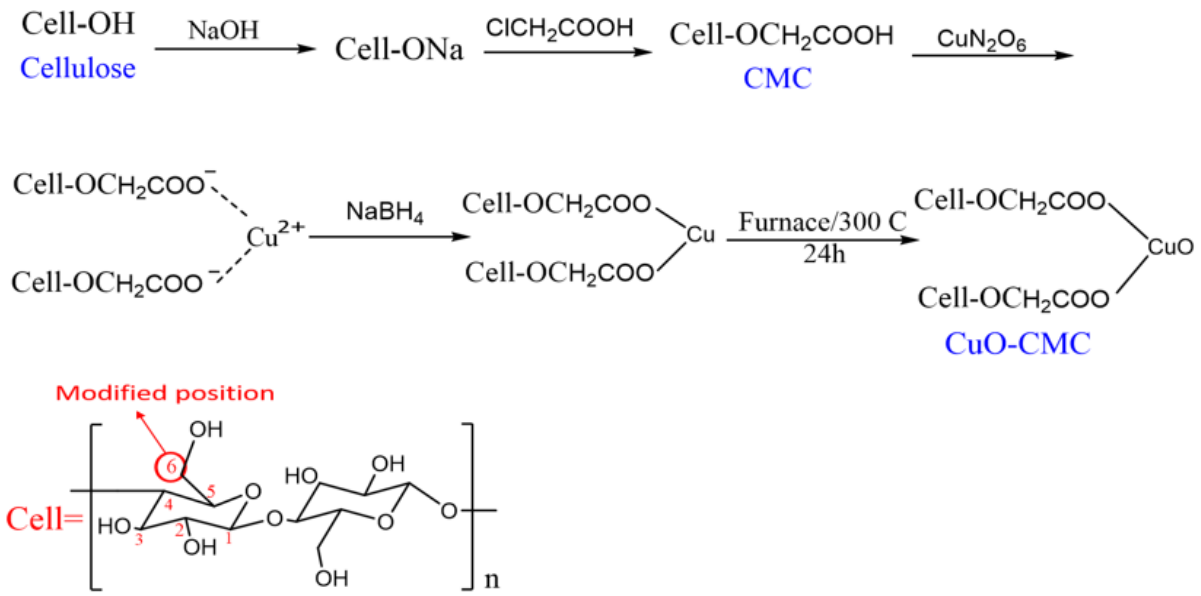

Fig. 1. Proposed reaction pathway for the synthesis of CuO-CMC nanocomposite

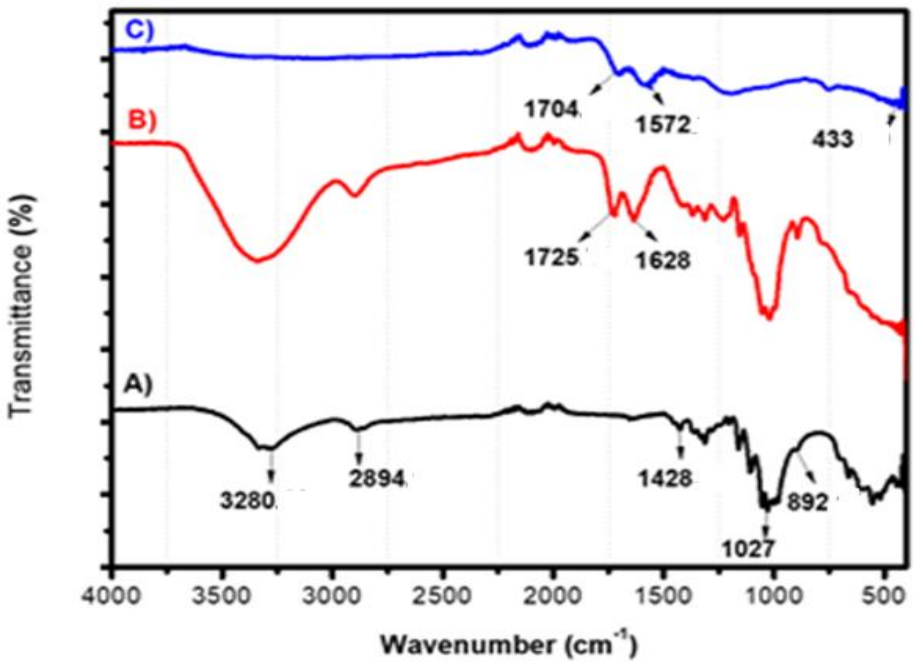

Fig. 2. FT-IR analysis of the A) Cellulose, B) CMC and C) CuO-CMC nanocomposites

amorphous areas, but also some crystalline areas [48]. Extra heating showed that from 380°C to 450°C the weight loss (DTGA curve) and residual weight of CuO/CMC and CMC was found to be higher compare to pure cellulose, this is maybe owing to the existence of crystalline cellulose polymorph which is basically heated renitent [48]. In observation of the aforementioned data, it was established that the CMC and CuO/CMC nanocomposites have good thermal stability.

3.2.4 SEM and EDX analysis

Fig. 5 (A, B) shows the surface morphology and elemental composition of the synthesized nanocomposite. Fig. 4A demonstrates CMC with a rod shape with 10.80 µm of diameter. In addition, Fig. 4B displays a large change in the morphology of CMC due to the presence of both spherical shape and cubic shape of CuO NPs with a uniform distribution that covers the surface of CMC.

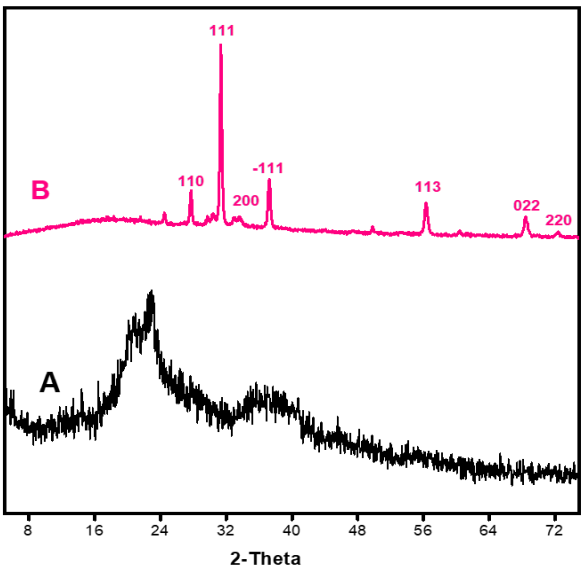

Fig. 3. XRD analysis of CMC and CuO-CMC nanocomposites

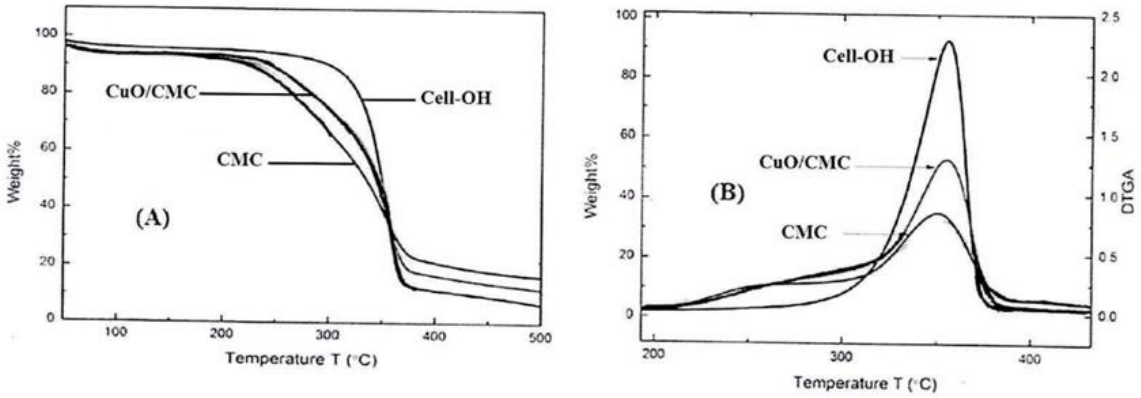

Fig. 4. TGA (A) and DTGA (B) curves for cellulose CuO/CMC nanocomposite and CMC

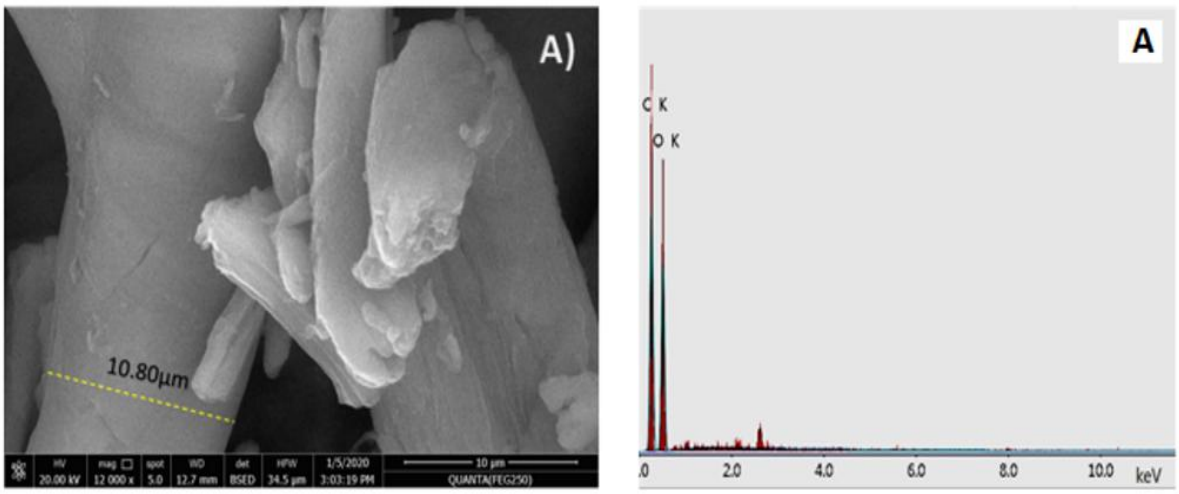

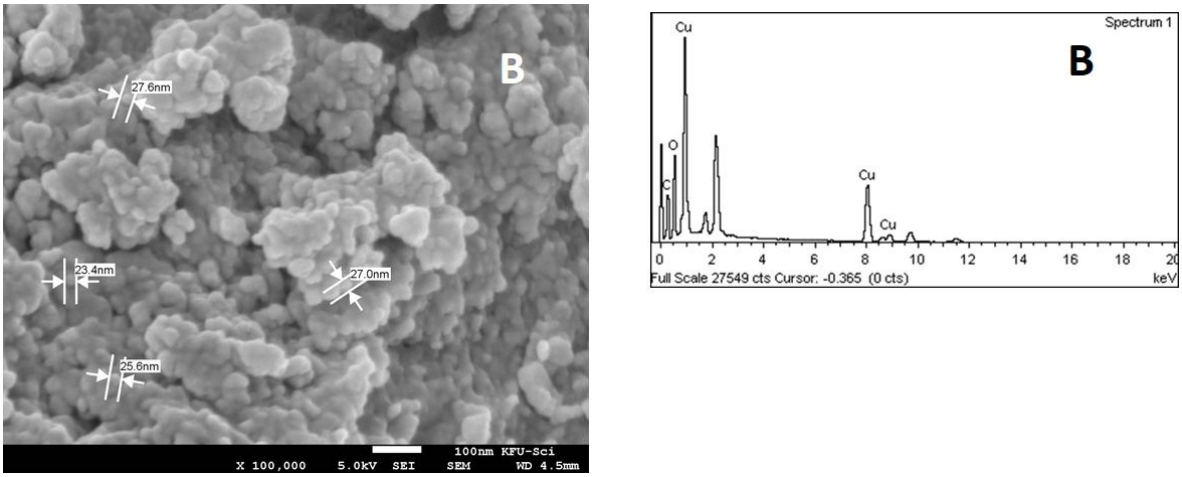

Fig. 5. SEM and EDX images of A) CMC and B) CuO-CMC

Furthermore, EDX spectral analysis clearly demonstrated the presence of CuO NPs in composite with the addition of the strong signal of oxygen and carbon at 8 and 9 KeV without any signal for contaminates.

3.2.5 TEM analysis

Fig. 6 shows the TEM images of CMC and CuO/CMC at high magnification power (500,000). Fig. 6A shows the image of CMC with a smooth surface without any traces of nanoparticles. The synthesized nanocomposite has particles in nano-size range, random distribution on the CMC surface, and a semi-spherical shape without any agglomerations has been shown as in Fig. 6B and C) at 100 and 50 nm scales also the particles displayed a size between 3 to 10 nm. To identify the crystal structure of nanocomposite the selected area diffraction (SAED) analysis was used as shown in Fig. 6D, it shows a small bright spot scattered around a bright circular central spot with different diameters which further confirmed the single crystalline form as suggested by the XRD pattern. Fig. 6F describes the histogram of the size of the nanoparticles into the CMC surface. Overall, 27.5% of nanoparticles have 4 nm size and 22.5% have 6 nm while the average size of the particles was found at 5.421 nm.

3.3 Adsorption of Methylene Blue at Different Parameters

3.3.1 Effect of contact time

Fig. 7 shows the effect of contact time (0-48 h) on the removal efficiency of MB by A) cellulose, B) CMC and C) CuO-CMC nanocomposite at 25^{o}C, using initial MB concentration 3 mg/L, the volume of solution 10 ml, pH 5.5, and adsorbent dose 2.5 mg. Fig. 7 A shows the removal efficiency of MB by native cellulose was increased from 1.6 to 4.6 % and becomes constant at first 30 min. While Fig. 6 B shows the removal efficiency of MB was increased to 6 % using CMC and becomes constant at the first 30 min. Fig. 6 C shows the removal efficiency of MB was increased to 100 % when CuO-CMC nanocomposites were used and this attributed to the rapid adsorption and reduction of MB molecules on the nanocomposite surface in an aqueous medium [38]. Furthermore, it was accounted for that CuO NPs indicated amazing synergist action and selectivity on numerous catalytic reactions [49]. Considering the experimenting outcomes, one can recommend that the removal of dye in water followed the mechanism of both catalytic reduction and physical adsorption [50,51]. After MB adsorption, BET surface area analysis data of CuO/CMC nanocomposite was decreased from 80 m^2/g to 13 m^2/g, which attributed to the collection of MB on the surface of CuO/CMC nanocomposite. Moreover, at the beginning of the adsorption time at 1.5 h, it was observed that fast adsorption of MB occurred and this is attributed to the availability of available surface sites and carboxyl groups with a large surface area of the nanocomposite [52]. With increasing contact time, a little change in adsorption capacity occurred due to the lack of active sites on the material surface furthermore the removal efficiency of MB decreases with increases in contact time. In addition, through the adsorption process, the dye molecules migrated from an aqueous solution to the nanocomposite surface and then adsorbed by van der Waals force. Subsequently, the electrostatic interactions occurred when the cationic dye MB were close enough to the adsorption on the surface of CMC [53].

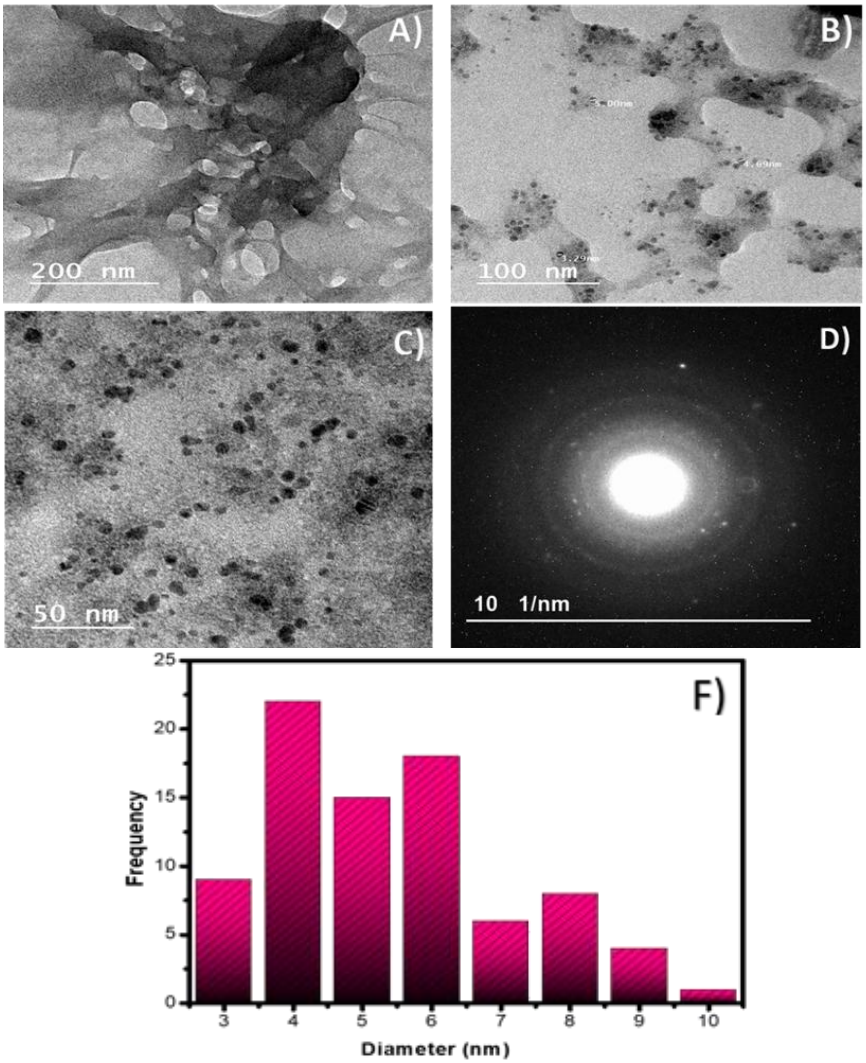

Fig. 6. TEM images of A) CMC, B and C) CuO/CMC at different magnification scales, D) SAED and F) Histogram of NPs size distribution

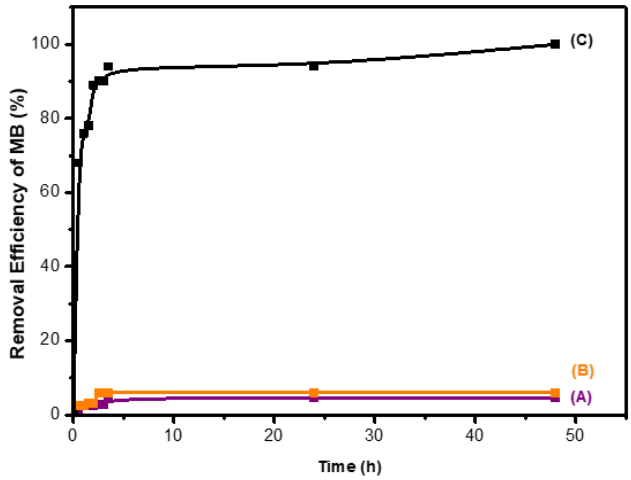

Fig. 7. The removal efficiency percent of MB using A) cellulose, B) CMC and C) CuO-CMC nanocomposites using initial MB concentration 3 mg/L, volume of solution 10 ml, pH 5.5, and adsorbent dose 2.5 mg at 25°C using different contact time (h).

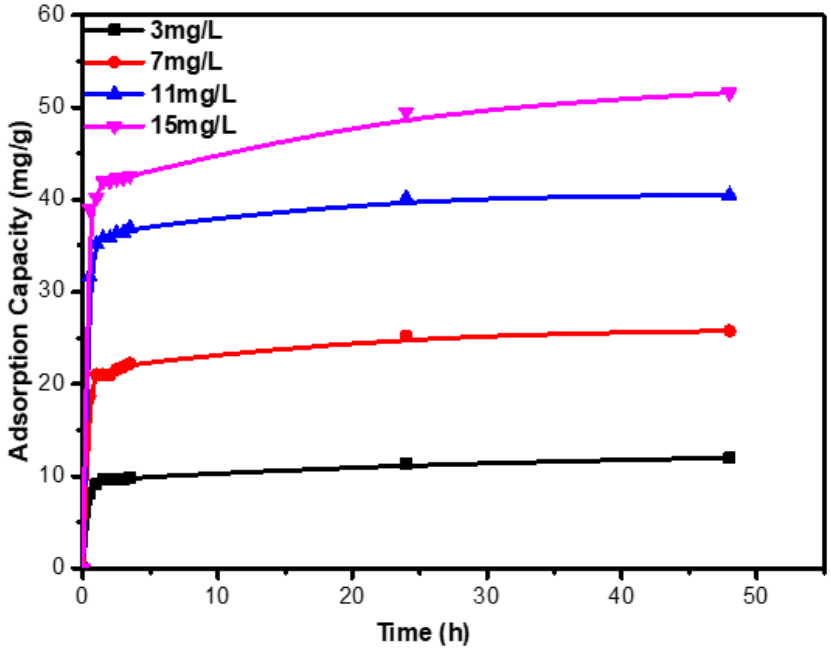

Fig. 8. Adsorption capacity (mg/g) of CuO-CMC nanocomposite using solution volume 10 ml, pH 5.5, and adsorbent dose 2.5 mg at 25°C for contact times (0-48 h) using different MB concentrations (3-15) mg/L.

3.2.2 Effect of MB concentrations

Fig. 8 shows the impact of the variety of the MB concentrations (3, 7, 11, and 15 mg) on the adsorption capacity of nanocomposite at 25oC, the volume of solution 10 ml, pH 5.5, adsorbent dose 2.5 mg. The data show that the adsorption capacity of CuO-CMC gradually increases with an increase in the dye concentration during the first hour until the equilibrium at 1.5 h. This is attributed to the plenty sites on the surfaces of nanocomposite then, it is slightly changed because the ions of methylene blue are looking to find available adsorption sites and once all the vacant adsorption sites of CuO-CMC nanocomposite had been occupied by MB molecules [53]. The values of adsorption capacity at 1.5 h (9, 21, 35.8, and 42) mg/g for initial concentration MB (3, 7, 11, and 15) mg/L, respectively. When the contact time is more than 1.5 h a little change in adsorption capacity is observed [53].

3.2.3 Effect of temperature

Temperature is a significant parameter in an adsorption procedure and the impact of temperature on the evacuation of MB was researched as appeared in (Fig. 9), at (25, 35, 45, 55, and 65°C), contact time 1.5 h, initial concentration of MB 3 mg/L, the volume of solution 10 ml, pH 5.5, adsorbent dose 2.5 mg. The data delineated that, when the temperature extended from 25 to 65°C, the removal efficiency of MB increased from 57 to 86 %. This attributed to the increase in the mobility and diffusion of MB dye in solution, then an increase in the interaction between MB molecules and the active site of the adsorbent [20]. According to the adsorption of thermodynamic data, the ΔH° value was positive which indicated that the adsorption processes of MB onto CuO-CMC nanocomposite are endothermic in nature.

3.2.4 Effect of CuO-CMC nanocomposite dosage

Several dosages from (2 to 10 mg) of adsorbent were applied to investigate the effect of adsorbent amount on the removal of MB dye, at 25°C, contact time 1.5 h, initial concentration of MB 3 mg/L, the volume of solution 10 ml, pH 5.5. Fig. 10 shows the removal efficiency percentage of MB increases with increase the adsorbent dosage from 2 to 8 mg and becomes constant at 10 mg, it is approximately 97 %. This attributed to the abundance of active sites for adsorption and increase of the surface area of the adsorbent. In contrast, the adsorption capacity decreased from 11 to 3.56 (mg/g). The removal efficiency and adsorption capacity were not changed when the adsorbent dosages were more than 8 mg. This phenomenon occurs due to an aggregation of adsorbent so this will reduce the surface area and active sites. The trend of results was similar with Ghulam et al. [21].

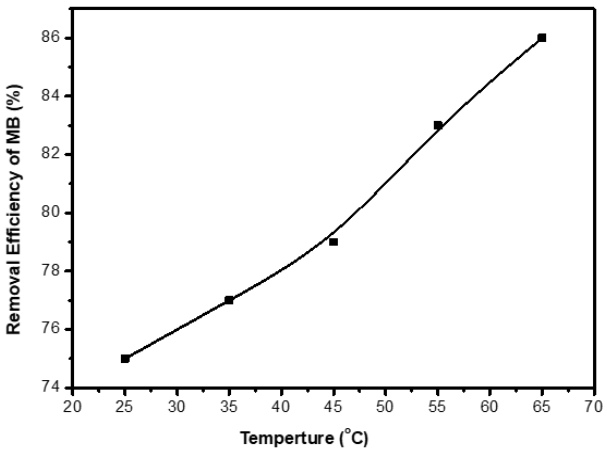

Fig. 9. Removal efficiency of MB using 2.5 mg of CuO-CMC nanocomposite, initial concentration of MB 3 mg/L, volume of solution 10 ml, contact time 1.5 h, pH 5.5, at different temperature (25-65°C).

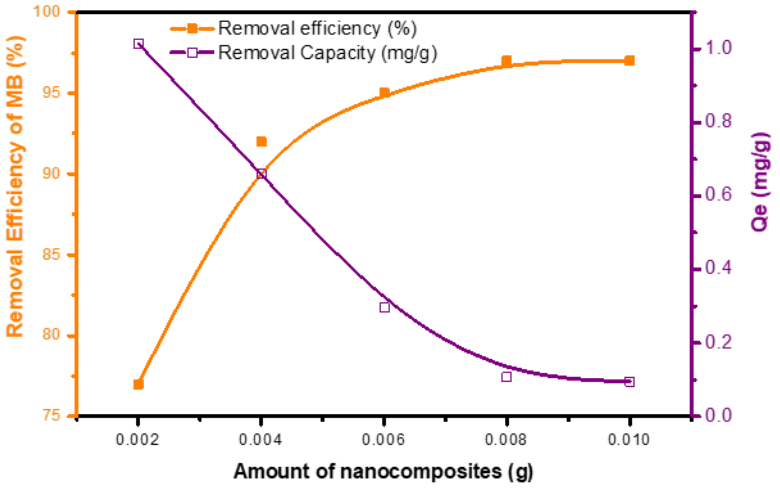

Fig. 10. Removal efficiency of MB and removal capacity (mg/g) using initial concentration of MB 3 mg/L, volume of solution 10 ml, contact time 1.5 h, pH 5.5 at 25°C using different dosage of CuO-CMC nanocomposite

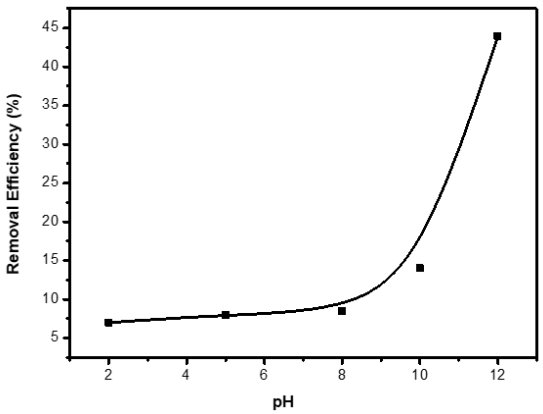

Fig. 11. MB removal efficiency using 2.5 mg of CuO-CMC nanocomposite with initial MB concentration 3 mg/L, volume of solution 10 ml, contact time 1.5 h, at 25°C using different pH.

Table 1. Kinetic data of MB adsorption onto CuO-CMC nanocomposite

	Pseudo 1st order		Pseudo 2nd order	
C_o (mg/L)	k_1 (h^{-1})	R^2_1	K_2 (L/mg.h)	R^2_2
0.5	0.072	0.599	0.189	0.949
1	0.054	0.493	0.041	0.844
1.5	0.051	0.231	0.029	0.864
2	0.049	0.496	0.008	0.626

3.2.5 Effect of pH

Fig. 11 shows the impact of shifting the adsorption pH (2-12) on the adsorption parameters at 25°C, contact time 1.5 h, initial concentration of MB 3 mg/L, the volume of solution 10 ml, adsorbent dose 2.5 mg. Expanding the adsorption pH positively affects the MB evacuation rate. The MB removal rate increases from 7% to 44%. The straight and moderate addition is watched for a pH range of 2 to 8, at that point the fast exponential increment is identified. The veiling impact of the first positive charges over the nanocomposite has diminished because of the alkaline medium and empowers the negative ones from the nanocomposite to be pulled into the positively charged MB molecules [54].

3.3 Adsorption Kinetics

Adsorption kinetics is important to characterize the adsorption process between the Liquid-Solid interfaces. In general, to confirm the best effective model two kinetic models were applied, pseudo 1st order and pseudo 2nd order. The linear form of the pseudo 1st order kinetic model can be expressed as the following equation (5) [55]:

$$\ln C_t/C_o = -kt \quad (5)$$

where C_o is the initial concentration, C_t is the residual concentration of MB (mg/L) at a definite time t (h) and k_1 is the rate constant for pseudo 1st order (h^{-1}), which can be calculated from plotting of ln C_t/C_o versus time as shown in Fig. 12A. While the linear form of the pseudo 2nd order model is represented as the following equation (6) [56]:

$$1/C_t = 1/C_o + k_2 t \quad (6)$$

where k_2 is the rate constant for pseudo 2nd order (L/mg.h) which, can be calculated from a plot of $1/C_t$ versus time as shows in Fig. 12B. (Table 1) summarizes the values of the rate constants and the correlation coefficients for pseudo 1st and pseudo 2nd order. According to Fig. 12 and Table 1, it clear that the applicable model for describing the adsorption of MB by the synthesized material was the pseudo 2nd order, which is consistent with a previous report by Hatem et al. [20]. The correlation coefficient values (R^2_2=0.949, 0.844, 0.8764 and 0.626) were found to be higher than those of the pseudo 1st order (R^2_1= 0.519, 0.413, 0.231 and 0.416). Obviously, the values of rate constants decrease gradually with increases of initial concentration of the MB duo to the active sites of nanocomposite. According to the above results, the adsorption of BM ($[C16_6H_{18}\ N_3S]^+$) cationic onto $[CuO\text{-}CMC]^-$ anionic in aqueous solution is chemisorption which occurred by transfer, exchange or sharing electrons [57].

3.4 Adsorption Isotherms

Distinctive isotherm models characterize the adsorption technique utilized. The most punctual utilized one is the Freundlich isotherm, which proposes that the adsorbent surface has heterogeneous site energies and multi-layers of sorption. Nevertheless, the Langmuir isotherm accepts a totally homogeneous surface with a limited indistinguishable number of locales, however, disregards the collaboration between the adsorbed particles and results in monolayer sorption [58, 59]. Equations (7) and (8) can express the linearized Langmuir and Freundlich isotherms respectively as following:

$$\frac{C_e}{Q_e} = \frac{1}{q_{max}} C_e + \frac{1}{q_{max} K_L} \quad (7)$$

.

where, C_e is the concentration of MB at equilibrium (mg/L), q_{max} is the theoretical maximum monolayer adsorption capacity of the adsorbent (mg/g) and K_L is the constant of Langmuir (L/mg). The values of q_{max} and K_L are determined from the plot between C_e/Q_e and C_e.

$$\ln Q_e = \ln k_F + 1/n \ln C_e \quad (8)$$

Where K_F is the Freundlich constant (L/mg) which is represented the affinity of the adsorbate for the adsorbent and 1/n is the intensity of adsorption that is related to the multiplicity and heterogeneity of the surface, which are evaluated from the linear plot between ln Q_e and ln C_e. The type of the isotherm R_L was determined according to the following equation:

$$R_L = \frac{1}{1 + k_L C_o} \quad (9)$$

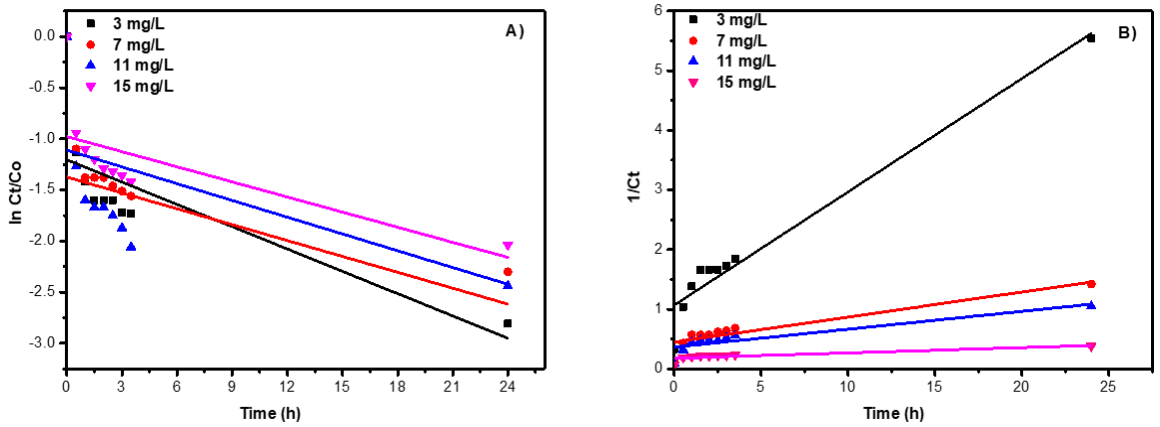

Fig. 12. Plots for the behaviour of adsorption MB, A) pseudo 1st order and B) pseudo 2nd order kinetics.

Table 2. Isotherm adsorption parameters at 338 K

Isotherm model	Langmuir				Freundlich		
Parameters	**q_{max} (mg/g)**	**K_L (L/mg)**	**R_L**	**R^2**	**$1/n$**	**k_F (L/mg)**	**R^2**
Result	100	0.188	0.261	0.933	0.913	2.512	0.736

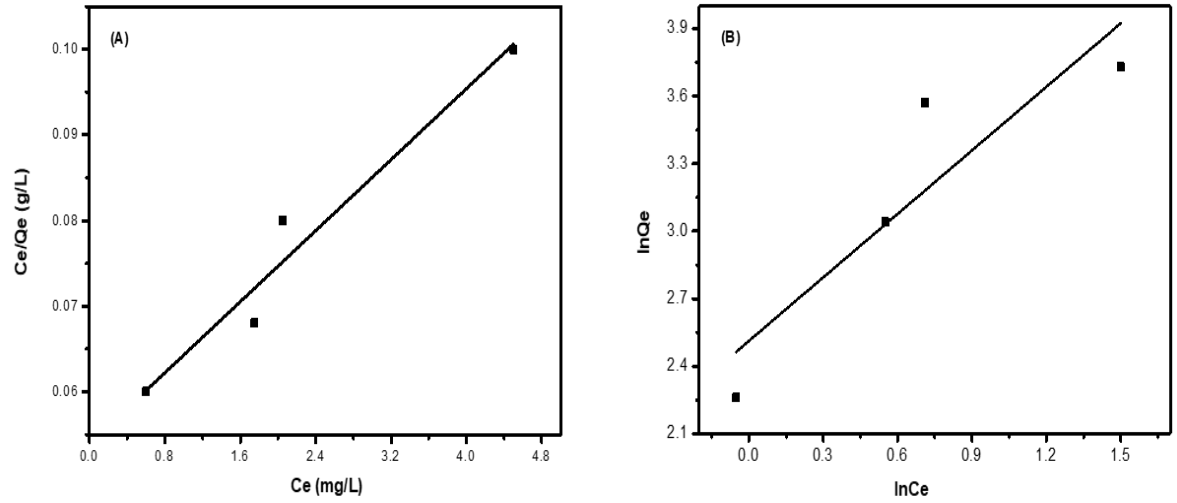

Fig. 13. Isotherm plots for A) Langmuir and B) Freundlich model at 338 K

According to Fig. 13A and 13B and, the fitting parameters in Table 2. The data show that the correlation coefficient value in the Langmuir model (R^2) equal to 0.933) which, is higher than that the correlation coefficient value in the Freundlich model (R^2) which, equal to 0.736) and the maximum adsorption capacity of adsorbent (q_{max}) equal 100 mg/g. In addition, the values of *R*L and 1/n were 0.261 and 0.933, respectively. The high correlation coefficient (R^2 =0.933) demonstrates that the adsorption of the MB onto CuO-CMC nanocomposite fully obeyed the Langmuir isotherm.

3.5 Adsorption Thermodynamics

To investigate the adsorption mechanism of CuO-CMC nanocomposite, the thermodynamic parameters including Gibbs free energy change ΔG^o (kJ/mole), enthalpy change ΔH^o (kJ/mole) and entropy change ΔS^o (J/K. mole) were estimated by the thermodynamic formulas as shown in the equations (10) and (11) [60]:

$$\ln K_d = \frac{\Delta S^\circ}{R} - \frac{\Delta H^\circ}{RT} \qquad (10)$$

$$\Delta G^o = -RT \ln K_d \quad (11)$$

where T is the system temperature (Kelvin), R is the gas constant (8.314 J/K. mole) and K_d is the equilibrium rate constant (L/g). The K_d value was calculated according to reported method as the following equation (12) (Kuang et al., 2020):

$$K_d = \frac{Q_e}{c_e} \quad (12)$$

The ΔH^o and ΔS^o can be obtained from the slope and intercept of the lines between $\ln K_d$ and 1/T as shown in Fig. 14 and the obtained results of thermodynamic parameters are listed in Table 3. The data show that the K_d values increases from 14.879 to 30.569 (L/g) with increase of the temperature from 298 to 338 (K) and the all values of ΔG^o are negative in the all studied temperature. This confirmed that the adsorption process is spontaneous. Furthermore, the value of ΔH^o was in a positive (1.82 kJ/mole) which demonstrates that the adsorption process is endothermic. Another observation, the positive values of (ΔS^o=8.65 J/K. mole) during the adsorption process due to the randomness of the solid-solution interface, when the active sites of nanocomposite combined with MB molecule in aqueous solution [61].

Table 4 shows the comparative study of adsorption capacity of prepared CuO/CMC nanocomposite with some reported adsorbents such as activated carbon lignin-chitosan, Brown macroalga, and chitosan/ graphene oxide, Graphene oxide/ lignosulfonate aerogel cross-linked by chitosan (GLCA). As recorded in Table 4, the CuO/CMC nanocomposite influenced a greater adsorption capacity against MB than the described adsorbents, containing brown macroalga, chitosan/GO, activated carbon, and lignin-chitosan, while less than GLCA adsorbent. While such a comparison is not being impartially adequate

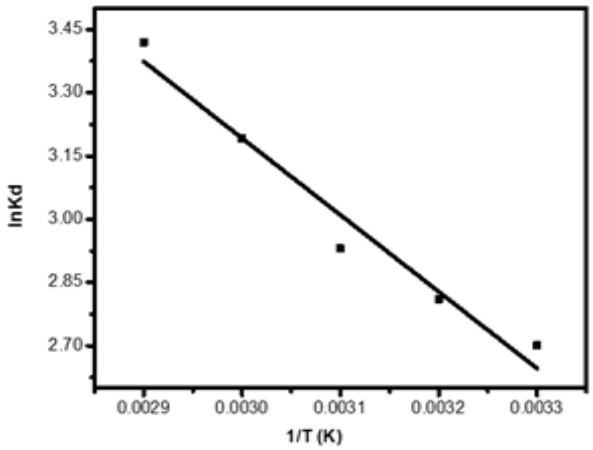

Fig. 14 Thermodynamic plot for MB adsorption

Table 3. Estimated parameters of thermodynamic adsorption

(K)Temperature	K_d	ΔG^o (kJ/mol)	ΔH^o (kJ/mol)	ΔS^o (kJ/mol.K)
298	14.879	-6.68	1.82	8.65
308	16.739	-7.19		
318	18.809	-7.74		
328	24.411	-8.69		
338	30.569	-9.60		

Table 4. Comparative study between the adsorption capacity of CuO/CMC and some reported adsorbents

Adsorbent	Adsorption capacity (mg/g)	pH	T (K)	Reference
Activated carbon	91.0	7	301	(Yener et al., 2008) [62]
Lignin-chitosan	36.3	7	293	(Albadarin et al., 2017) [63]
Brown macroalga	95.5	6.5	300	(Daneshvar et al., 2017) [64]
Chitosan/GO	95.2	5.3	303	(Fan et al., 2012) [65]
GLCA	1023.9	7.0	303	(Mingfang et al., 2019) [66]
CuO-CMC	100	5.5	338	This study

because of the alteration in the conditions of the experiment. The stated adsorption capacities recommended that the obtained CuO/CMC nanocomposite could be more economical than the other adsorbents because cellulose is present in a large amount in many natural sources, and it can be obtained in many cheap ways. Also, the composites based on cellulose in an easy and inexpensive way, make it used to remove pollutants from water.

4. CONCLUSION

CuO-CMC nanocomposite was successfully synthesized by the co-precipitation method with thermal treatment, which is exhibiting a high loading yield of metal oxides onto the backbone of the CMC structure. Notably, the synthesized nanocomposite was exhibited high performances for removing cationic dye (MB) from an aqueous solution. FT-IR, XRD, SEM, EDX, TEM are physicochemical tools that used to characterize the prepared nanocomposite. FT-IR and XRD pattern showed that the presence of (COO) group and Cu-O bond and the crystallinity of CMC was damaged after generated CuO NPs on its surface. SEM and EDX analysis showed that the rough surface of CMC due to the precipitation of the CuO NPs which cover all of the surfaces. Moreover, TEM analysis confirmed that the synthesized nanocomposite has particles in nano-size range (3-10 nm), random distribution, and a semi-spherical shape with a few tendencies of agglomerations. The factors affecting the adsorption capacity and removal efficiencies, such as the initial concentration of MB, contact time, temperature, adsorbent dosage, and solution pH were studied. The results showed that these factors affected positively. The adsorption capacities of MB on CuO-CMC were (12, 25.76, 40.48, and 51.63) for initial concentration (3, 7, 11, and 15 mg/L) after 48 h. The experimental results agreed well with the Langmuir isotherm model with a maximum adsorption capacity (q_{max} = 100 mg/g) and the pseudo 2nd order kinetics based on the correlation coefficients (R^2) values which are higher than pseudo 1st order. In addition, the thermodynamic parameters were indicated a spontaneous and endothermic process for MB dye adsorption due to the negative values of ΔG^o and positive of ΔH^o, respectively. Finally, these results recommended that the CuO-CMC nanocomposite possesses are excellent potential to be applied as an adsorbent in the water treatment with good efficient, environmentally friendly, and inexpensive materials. Furthermore, this nanocomposite has been examined for corrosion preventing features and the results showed that CuO-CMC nanocomposite were efficient inhibitors for carbon-steel corrosion in acidic medium [67].

ACKNOWLEDGEMENTS

The authors would like to thank the Chemistry Department, College of Science, King Fasil University for its supporting and offering to finish this work.

DATA AVAILABILITY STATEMENTS

The datasets investigated during the examination are accessible from the corresponding author on solicitation.

DECLARATION OF INTEREST

The authors declare that they have no known competing financial interests or personal relationships that could have appeared to influence the work reported in this paper.

COMPETING INTERESTS

Authors have declared that no competing interests exist.

REFERENCES

1. Hamid N, Li T. Degradation of methylene blue using CuO prepared using conventional solid state method. Journal of Engineering and Technology (JET). 2019;10.
2. Hemaviboon K, Klamtet J. Removal of methylene blue dye from aqueous solution by adsorption on leonardite char. Naresuan University Journal: Science and Technology (NUJST). 2020;28:82-93.
3. Tang S, Wang Z, Yuan D, Zhang Y, Qi J, Rao Y, Lu G, Li B, Wang K, Yin K. Enhanced photocatalytic performance of $BiVO_4$ for degradation of methylene blue under LED visible light irradiation assisted by peroxymonosulfate. International of Electrochemical Science. 2020;15:2470-2480. DOI:https://doi.org/10.20964/2020.03.09
4. El Nemr A, Hassaan MA, Madkour FF. Advanced oxidation process (AOP) for detoxification of acid red 17 dye solution and degradation mechanism. Environmental Processes. 2018;5:95-113. DOI:https://doi.org/10.1007/s40710-018-0284-9
5. Le TTH, Phung BQ, Dang DD. Synthesis of $Bi_{0.5}Li_{0.5}TiO_3$ nanoparticles by Sol-Gel method for photocatalytic methylene blue degradation and antibacterial activity. Journal of Nanomaterials; 2019.

DOI:https://doi.org/10.1155/2019/5784610.

6. Lau YY, Wong YS, Teng TT, Morad N, Rafatullah M, Ong SA. Degradation of cationic and anionic dyes in coagulation–flocculation process using bi-functionalized silica hybrid with aluminum-ferric as auxiliary agent. RSC Advances. 2015;5:34206-34215.
   DOI:https://doi.org/10.1039/c5ra01346a.
7. Ashraf, M.W, 2016. Removal of methylene blue dye from wastewater by using supported liquid memberane technology. Polish Journal of Chemical Technology 18, 26-30. DOI:https://doi.org/10.1515/pjct-2016-0025.
8. Yu Z, Hu C, Dichiara AB, Jiang W, Gu J. Cellulose nanofibril/carbon nanomaterial hybrid aerogels for adsorption removal of cationic and anionic organic dyes. Nanomaterials. 2020;10:169-188.
   DOI:https://doi.org/10.3390/nano10010169.
9. Wei W, Yang L, Zhong W, Li S, Cui J, Wei Z. Fast removal of methylene blue from aqueous solution by adsorption onto poorly crystalline hydroxyapatite nanoparticles. Dig. J. Nanomater. Biostruct. 2015;19:1343-1363.
10. Kuang Y, Zhang X, Zhou S. Adsorption of methylene blue in water onto activated carbon by surfactant modification. Water. 2020;12: 587-605.
    DOI:https://doi.org/10.3390/w12020587.
11. Narayanaswamy V, Kumar H, Srivastava C, Alaabed S, Aslam M, Mallya A, Obaidat IM. Adsorption of methylene blue and rhodamine B on graphene oxide-Fe_3O_4 nanocomposite: Molecular dynamics and Monte Carlo simulations. Materials Express. 2020;10:314-324.
    DOI:https://doi.org/10.1166/mex.2020.1647.
12. Manjari G, Saran S, Arun T, Rao AVB, Devipriya SPJJoSCS. Catalytic and recyclability properties of phytogenic copper oxide nanoparticles derived from Aglaia elaeagnoidea flower extract. 2017;21:610-618. DOI:http://dx.doi.org/10.1016/j.jscs.2017.02.004
13. Goyal CP, Goyal D, Rajan K, S, Ramgir NS, Shimura Y, Navaneethan M, Hayakawa Y, Muthamizhchelvan C, Ikeda H, Ponnusamy SJC. Effect of Zn doping in CuO octahedral crystals towards structural. Optical, and Gas Sensing Properties. 2020;10:188-204. DOI:https://doi.org/doi:10.3390/cryst10030188.
14. Kanwar R, Bhar R, Mehta SKJC. Designed meso macroporous silica framework impregnated with copper oxide nanoparticles for enhanced catalytic performance. 2018;10: 2087-2095.
    DOI:https://doi.org/10.1002/cctc.201701630.
15. Manasrah AD, Almanassra IW, Marei NN, Al-Mubaiyedh UA, Laoui T, Atieh MA. Surface modification of carbon nanotubes with copper oxide nanoparticles for heat transfer enhancement of nanofluids. RSC Advances. 2018;8:1791-1802.
    DOI:https://doi.org/10.1039/c7ra10406e.
16. Davarpanah SJ, Karimian R, Piri F.. Synthesis of copper (II) oxide (CuO) nanoparticles and its application as gas sensor. Journal of Applied Biotechnology Reports. 2015;2:329-332.
17. Paulose R, Raja M. CuO nanoparticles/multi-walled carbon nanotubes (MWCNTs) nanocomposites for flexible supercapacitors. Journal of Nanoscience and Nanotechnology. 2019;19:8151-8156.
    DOI:https://doi.org/10.1166/jnn.2019.16874.
18. Hassan SED, Fouda A, Radwan AA, Salem SS, Barghoth MG, Awad MA, Abdo AM, El-Gamal MS. Endophytic actinomycetes Streptomyces spp mediated biosynthesis of copper oxide nanoparticles as a promising tool for biotechnological applications. JBIC Journal of Biological Inorganic Chemistry. 2019;24: 377-393.
    DOI:https://doi.org/10.1007/s00775-019-01654-5.
19. Nwanya AC, Ndipingwi MM, Mayedwaa N, Razanamahandry L, Ikpo CO, Waryo T, Ntwampe S, Malenga E, Fosso-Kankeu E, Ezema FI. Maize (*Zea mays* L.) fresh husk mediated biosynthesis of copper oxides: Potentials for pseudo capacitive energy storage. Electrochimica Acta. 2019;301:436-448.
20. Al-Aoh HA, Mihaina IA, Alsharif MA, Darwish A, Rashad M, Mustafa SK, Aljohani MM, Al-Duais MA, Al-Shehri H. Removal of methylene blue from synthetic wastewater by the selected metallic oxides nanoparticles adsorbent: equilibrium, kinetic and thermodynamic studies. Chemical Engineering Communications. 2019;1-17.
    DOI:https://doi.org/10.1080/00986445.2019.1680366.
21. Mustafa G, Tahir H, Sultan M, Akhtar N. Synthesis and characterization of cupric oxide (CuO) nanoparticles and their application for the removal of dyes. African Journal of Biotechnolog. 2013;12:6650-6660.
    DOI:https://doi.org/10.5897/AJB2013.13058.
22. Lu H, Zhang L, Ma J, Alam N, Zhou X, Ni Y. Nano-cellulose/MOF derived carbon doped CuO/Fe_3O_4 nanocomposite as high efficient

catalyst for organic pollutant remedy. Nanomaterials. 2019a;9:277-288. DOI:https://doi.org/doi:10.3390/nano9020277.

23. Sapkota KP, Lee I, Hanif M, Islam M, Akter J, Hahn JR. Enhanced visible-light photocatalysis of nanocomposites of copper oxide and single-walled carbon nanotubes for the degradation of methylene blue. Catalysts. 2020;10:297312. DOI:https://doi.org/10.3390/catal10030297.
24. Saghian M, Dehghanpour S, Sharbatdaran M. Unique and efficient adsorbents for highly selective and reverse adsorption and separation of dyes via the introduction of SO_3H functional groups into a metal–organic framework. RSC Advances. 2020;10:9369-9377. DOI:https://doi.org/10.1039/c9ra10840h.
25. Jabbar SM. Synthesis of CuO nano structure via sol-gel and precipitation chemical methods. Al-Khwarizmi Engineering Journal. 2016;12: 126-131. DOI:http://dx.doi.org/10.22153/kej.2016.07.001.
26. Outokesh M, Hosseinpour M, Ahmadi S, Mousavand T, Sadjadi S, Soltanian W.. Hydrothermal synthesis of CuO nanoparticles: study on effects of operational conditions on yield, purity, and size of the nanoparticles. Industrial & Engineering Chemistry Research. 2011;50:3540-3554. DOI:https://doi.org/10.1021/ie1017089.
27. Barreca D, Comini E, Gasparotto A, Maccato C, Sada C, Sberveglieri G, Tondello E. Chemical vapor deposition of copper oxide films and entangled quasi-1D nanoarchitectures as innovative gas sensors. Sensors and Actuators B: Chemical. 2009;141:270-275. DOI:https://doi.org/10.1016/j.snb.2009.05.038.
28. Karthick Kumar S, Murugesan S, Suresh S, Paul Raj S. Nanostructured CuO thin films prepared through sputtering for solar selective absorbers. Journal of Solar Energy; 2013. DOI:http://dx.doi.org/10.1155/2013/147270.
29. Saimon JA, Mahdi RO, Khashan KS, Abdulameer FA. Preparation of CuO NPs by laser ablation in liquid for photodiodes. AIP Conference Proceedings. AIP Publishing LLC. 2020;020312. DOI:https://doi.org/10.1063/5.0000118.
30. Manyasree D, Peddi K, Ravikumar R. CuO nanoparticles: synthesis, characterization and their bactericidal efficacy. Int J Appl Pharmaceut. 2017;9:71-74. DOI:http://dx.doi.org/10.22159/ijap.2017v9i6.71757
31. Ito H, Sakata M, Hongo C, Matsumoto T, Nishino T. Cellulose nanofiber nanocomposites with aligned silver nanoparticles. Nanocomposites. 2018;4:167-177. DOI:https://doi.org/10.1080/20550324.2018.1556912.
32. Oyewo OA, Elemike EE, Onwudiwe DC, Onyango MS. Metal oxide-cellulose nanocomposites for the removal of toxic metals and dyes from wastewater. International Journal of Biological Macromolecules; 2020. DOI:https://doi.org/10.1016/j.ijbiomac.2020.08.074.
33. Hussain R, Aziz W, Abbas Ibrahim I. Antibacterial activity of CuO-cellulose nano rods depends on anew green synthesis (cotton). Journal of Nanostructures. 2019;9:761-767. DOI:https://doi.org/10.22052/JNS.2019.04.017.
34. Yue X, Huang J, Jiang F, Lin H, Chen Y. Synthesis and characterization of cellulose-based adsorbent for removal of anionic and cationic dyes. Journal of Engineered Fibers and Fabrics. 2019;14:1-10. https://doi.org/10.1177/1558925019828194.
35. Gago D, Chagas R, Ferreira LM, Velizarov S, Coelhoso I. A novel cellulose-based polymer for efficient removal of methylene blue. Membranes. 2020;10:13-19. DOI:https://doi.org/10.3390/membranes10010013.
36. Khalil MI, Abdel-Halim MG. Preparation of some starch-based neutral chelating agents. Carbohydrate Research. 2000;324:189-199. https://doi.org/10.1016/S0008-6215(99)00290-6.
37. Harrad MA, Boualy B, El Firdoussi L, Mehdi A, Santi C, Giovagnoli S, Nocchetti M, Ali, MA. Colloidal nickel (0)-carboxymethyl cellulose particles: A biopolymer-inorganic catalyst for hydrogenation of nitro-aromatics and carbonyl compounds. Catalysis Communications. 2013;32:92-100. DOI:http://dx.doi.org/10.1016/j.catcom.2012.11.025
38. Saikia P, MIAH T, A, Das PP. Highly efficient catalytic reductive degradation of various organic dyes by Au/ CeO_2-TiO_2 nano-hybrid. Journal of Chemical Sciences. 2017;129:81-93. DOI:https://doi.org/10.1007/s12039-016-1203-0.
39. Tasaso P. Optimization of reaction conditions for synthesis of carboxymethyl cellulose from oil palm fronds. International Journal of Chemical Engineering and Applications. 2015; 6:101-104.
40. Liu X, Lin B, Zhang Z, Lei H, Li Y. Copper (ii) carboxymethylcellulose (CMC-Cu II) as an efficient catalyst for aldehyde–alkyne–amine

coupling under solvent-free conditions. RSC Advances. 2016;6:94399-94407.

41. Bakhsh EM, Khan SA, Marwani HM, Danish EY, Asiri AM, Khan SB. Performance of cellulose acetate-ferric oxide nanocomposite supported metal catalysts toward the reduction of environmental pollutants. International Journal of Biological Macromolecules. 2018; 107:668-677. DOI:https://doi.org/10.1016/j.ijbiomac.2017.09.034.
42. Yáñez-S M, Matsuhiro B, Maldonado S, González R, Luengo J, Uyarte O, Serafine D, Moya S, Romero J, Torres R. Carboxymethylcellulose from bleached organosolv fibers of Eucalyptus nitens: synthesis and physicochemical characterization. Cellulose. 2018;25:2901-2914.
43. Sadanand V, Rajini N, Rajulu AV, Satyanarayana B. Preparation of cellulose composites with in situ generated copper nanoparticles using leaf extract and their properties. Carbohydrate Polymers. 2016;150: 32-39. DOI:http://dx.doi.org/10.1016/j.carbpol.2016.04.121
44. Wei X, Wang X, Gao B, Zou W, Dong L. Facile Ball-Milling Synthesis of CuO/Biochar Nanocomposites for Efficient Removal of Reactive Red 120. American Chemical Society. 2020;5:5748–5755. DOI:https://dx.doi.org/10.1021/acsomega.9b03787.
45. Alemdar A, Sain M. Biocomposite from wheat straw nanofibers: Morphology, thermal and mechanical properties. Composite Science and Technology. 2008;68:557–565.
46. Das K, Ray D, Bandyopadhyay N. R, Ghosh T, Mohanty AK, Misra M. A study of the mechanical, thermal and morphological properties of micro-crystalline cellulose particles prepared from cotton slivers using different acid concentrations. Cellulose. 2009; 16:783–793.
47. Jonoobi M, Khazaeian A, Tahir P, Azry SS, Oksman K. Characteris-tics of cellulose nanofibers isolated from rubberwood and empty fruit bunches of oil palm using chemo-mechanical process. Cellulose. 2011;18:1085–1095.
48. Mandal A, Chakrabarty D. Isolation of nanocellulose from waste sug-arcane bagasse (SCB) and its characterization. Carbohydrate Polymers. 2011;86:1291–1299.
49. Begum R, Najeeb J, Sattar A, Naseem K, Irfan, A, Al-Sehemi AG, Farooqi ZH. Chemical reduction of methylene blue in the presence of nanocatalysts: a critical review. Reviews in Chemical Engineering; 2019. DOI:https://doi.org/10.1515/revce-2018-0047.
50. Patel AC, Li S, Wang C, Zhang W, Wei Y. Electrospinning of porous silica nanofibers containing silver nanoparticles for catalytic applications. Chem Mater. 2007;19:1231–1238.
51. Chi Y, Zhao L, Yuan Q, Li Y, Zhang J, Tu J, Li N, Li X. Facile encapsulation of monodispersed silver nanoparticles in mesoporous compounds. Chem Eng J. 2012; 195–196:254–260.
52. Liu L, Gao ZY, Su XP, Chen X, Jiang L, Yao JM. Adsorption removal of dyes from single and binary solutions using a cellulose-based bioadsorbent. ACS Sustainable Chemistry & Engineering. 2015;3:432-442.
53. Yan M, Huang W, Li Z. Chitosan cross-linked graphene oxide/lignosulfonate composite aerogel for enhanced adsorption of methylene blue in water. International Journal of Biological Macromolecules. 2019;136:927-935. DOI:https://doi.org/10.1016/j.ijbiomac.2019.06.144.
54. Xu P, Zeng GM, Huang DL, Feng CL, Hu S, Zhao MH, Lai C, Wei Z, Huang C, Xie GX. Use of iron oxide nanomaterials in wastewater treatment: a review. Science of the Total Environment. 2012;424:1-10. DOI:https://doi.org/10.1016/j.scitotenv.2012.02.023.
55. Lu Q, Zhang Y, Hu H, Wang W, Huang Z, Chen D, Yang M, Liang J. In situ synthesis of a stable Fe_3O_4 @ cellulose nanocomposite for efficient catalytic degradation of methylene blue. Nanomaterials. 2019b;9:275-290. DOI:https://doi.org/10.3390/nano9020275.
56. Singh J, Chang YY, Koduru JR, Yang JK, Singh J, Chang YY, Koduru JR, Yang JK. Potential degradation of methylene blue (MB) by nano-metallic particles: A kinetic study and possible mechanism of MB degradation. Environmental Engineering Research. 2017; 23:1-9. DOI:https://doi.org/10.4491/eer.2016.158.
57. Ghasemi M, Mashhadi S, Azimi-Amin J. Fe_3O_4/AC nanocomposite as a novel nano adsorbent for effective removal of cationic dye: Process optimization based on Taguchi design method, kinetics, equilibrium and thermodynamics. Journal of Water and Environmental Nanotechnology. 2018;3:321-336.

DOI:https://doi.org/10.22090/jwent.2018.04.005.

58. Ayawei N, Ebelegi AN, Wankasi D. Modelling and interpretation of adsorption isotherms. Journal of Chemistry. 2017;1-11. DOI:https://doi.org/10.1155/2017/3039817.
59. Cheng J, Zhan C, Wu J, Cui Z, Si J, Wang Q, Peng X, Turng LS. Highly efficient removal of methylene blue dye from an aqueous solution using cellulose acetate nanofibrous membranes modified by polydopamine. American Chemical Society. 2020;5:5389–5400. DOI:https://dx.doi.org/10.1021/acsomega.9b04425.
60. Bouhdadi R, Benhadi S, Molina S, George B, El Moussaouiti M, Merlin A. Chemical modification of cellulose by acylation: Application to adsorption of methylene blue. Maderas. Ciencia y Tecnología. 2011;13:105-116. DOI:https://doi.org/10.4067/S0718-221X2011000100009.
61. Jin HX, Xu HP, Wang N, Yang LY, Wang YG, Yu D, Ouyang XK. Fabrication of carboxymethylcellulose/metal-organic framework beads for removal of Pb (II) from aqueous solution. Materials. 2019;12:942. DOI:https://doi.org/doi:10.3390/ma12060942.
62. Yener J, Kopac T, Dogu G, Dogu T. Dynamic analysis of sorption of Methylene Blue dye on granular and powdered activated carbon. Chemical Engineering Journal. 2008;144:400-406. DOI:https://doi.org/10.1016/j.cej.2008.02.009.
63. Albadarin AB, Collins MN, Naushad M, Shirazian S, Walker G, Mangwandi C. Activated lignin-chitosan extruded blends for efficient adsorption of methylene blue. Chemical Engineering Journal. 2017;307:264-272. DOI:https://doi.org/10.1016/j.cej.2016.08.089.
64. Daneshvar E, Vazirzadeh A, Niazi A, Kousha M, Naushad M, Bhatnagar A. Desorption of methylene blue dye from brown macroalga: effects of operating parameters, isotherm study and kinetic modeling. Journal of Cleaner Production. 2017;152:443-453. DOI:https://doi.org/10.1016/j.jclepro.2017.03.119.
65. Fan L, Luo C, Li X, Lu F, Qiu H, Sun M. Fabrication of novel magnetic chitosan grafted with graphene oxide to enhance adsorption properties for methyl blue. Journal of Hazardous Materials. 2012;215:272-279. DOI:https://doi.org/10.1016/j.jhazmat.2012.02.068.
66. Mingfang Y, Wenxing H, Zhili L. Chitosan cross-linked graphene oxide/lignosulfonate composite aerogel for enhanced adsorption of methylene blue in water. International Journal of Biological Macromolecules. 2019;136:927-935.
67. Abd El-Lateef HM, Albokheet W, Gouda M. Carboxymethyl cellulose/metal (Fe, Cu and Ni) nanocomposites as non-precious inhibitors of C-steel corrosion in HCl solutions: synthesis, characterization, electrochemical and surface morphology studies. Cellulose. 2020;27:8039-8057. DOI:https://doi.org/10.1007/s10570-020-03292-.